Photon-atom scattering of 13.95-, 17.75-, 26.36-, and 59.54-keV photons by Cu, Zn, Zr, Nb, Mo, Ag, Cd, In, Sn, Ta, and W

Ibrahim S. Elyaseery, A. Shukri, C. S. Chong, and A. A. Tajuddin
School of Physics, Universiti Sains Malaysia, 11800 USM Penang, Malaysia

D. A. Bradley
Physics Department, University of Malaya, 50603 Kuala Lumpur, Malaysia
(Received 22 August 1996; revised manuscript received 23 April 1997)

Differential coherent scattering cross sections for 11 moderate- to high-atomic-number elements have been experimentally determined with $O(10\%)$ error at the photon energies 13.95, 17.75, 26.36, and 59.54 keV, corresponding to major photon-emission intensities of the radionuclide ^{241}Am. The measurements were performed using a standard backscattering geometry setup to obtain scattering angles of 145°, 154°, and 165°, with resulting photon momentum transfers in the range $1.07 \leqslant x \leqslant 4.76$ Å^{-1}. High-purity (better than 99%) foils of Cu, Zn, Zr, Nb, Mo, Ag, Cd, In, Sn, Ta, and W were used as targets. A hyperpure germanium detector completed the arrangement. Measurements for Mo and Zr using the 17.75-keV photon-energy emission of ^{241}Am were not possible due to the fact that for these targets at this photon energy, intense fluorescence overlapped significantly with the coherent scatter. At 26.36 keV the coherent scatter from Cd was similarly dominated by fluorescence. Experimental data have been compared with predictions from relativistic form factors (RFFs), modified relativistic form factors (MRFFs), and counterpart RFF and MRFF approximations with anomalous corrections using angle-independent scattering factors. [S1050-2947(98)03104-7]

PACS number(s): 32.80.Cy, 32.90.+a, 25.20.Dc

I. INTRODUCTION

Measurements of differential coherent-scattering cross sections exist for high-Z elements, but less extensive data are available for medium- and low-Z elements, especially at photon energies of a few tens of keV or less [1,2]. This study addresses this situation and forms part of an ongoing investigation of elastic scattering by bound electrons for photon energies in the photon-energy interval from above 10 keV up to 60 keV. The impetus for this study derives from recently available theoretical calculations of anomalous scattering factors [3–5], there being a paucity of experimental data with which these predictions can be compared [6–12]. The aims of this present study are limited to obtaining results for elastic photon scattering for a number of low-, medium-, and high-Z elements having K edges close (within a few keV) to the exciting photon energies 13.95, 17.75, 26.36, and 59.54 keV emitted by the radionuclide ^{241}Am.

Experimental data for large-angle (beyond 130°) coherent scattering of 59.54-keV photons of ^{241}Am are already available in the literature from work carried out by earlier investigators. Schumacher and Stoffregen [13], for example, have measured coherent cross sections for six target elements within the range $30 < Z < 82$ at selected angles between 60° and 150°. Similar measurements with 59.54-keV photons on seven target elements at various angles between 60° and 165° have been carried out by Nandi, Dutta, and Chaudhuri [14], while Bui and Milazzo [9] have performed measurements on 24 target elements of $29 < Z < 92$ at 131°. Measurements by Varier and Unnikrishnan [15] have focused on seven target elements at 141.3°. All of these large-angle measurements with 59.54-keV photons have shown good agreement at their respective angles with theoretical S-matrix results. Measurements by Puri *et al.*[16] at 130° by 19 elements in the atomic region $13 \leqslant Z \leqslant 82$ have shown that for low-Z elements with the K-shell threshold below 59.54 keV, the measured scattering differential cross sections are in general agreement with form-factor approximations, whereas for high-Z elements, good agreement is observed with S-matrix calculations. We also note measurements for 59.54-keV photons coherently scattered at angles less than 130° measured by a number of other authors [17–21]. At 59.54 keV no measurements have been reported at the particular scattering angles 145°, 154°, and 165°, as investigated herein. Apart from these results for 59.54-keV photons there are presently no reported experimental data in the literature from other investigators for the other emissions of ^{241}Am.

II. EXPERIMENT

The basic experimental arrangement, described in detail elsewhere [22], provides for the detection of elastically scattered photons at backscattering angles. Measurements have been carried out using an annular ^{241}Am source of activity 3.7×10^9 Bq (100 mCi) (produced by Amersham International). It is to be noted that the radionuclide ^{241}Am emits photons over a wide range of energies, the most prominent of which are those at 13.95, 17.75, 26.36, and 59.54 keV.

Use has been made of an EG&G ORTEC planar high-purity germanium detector (crystal specifications: 10 mm detector active diameter, 3 mm thickness, 7 mm separation from window to front face of crystal) coupled to a microcomputer-based multichannel analyzer. At 59.54 keV a full width at half maximum of about 450 eV was maintained throughout the investigation.

The ^{241}Am source was housed in a stainless-steel holder, retaining a heavy tungsten alloy insert, capped with a thin

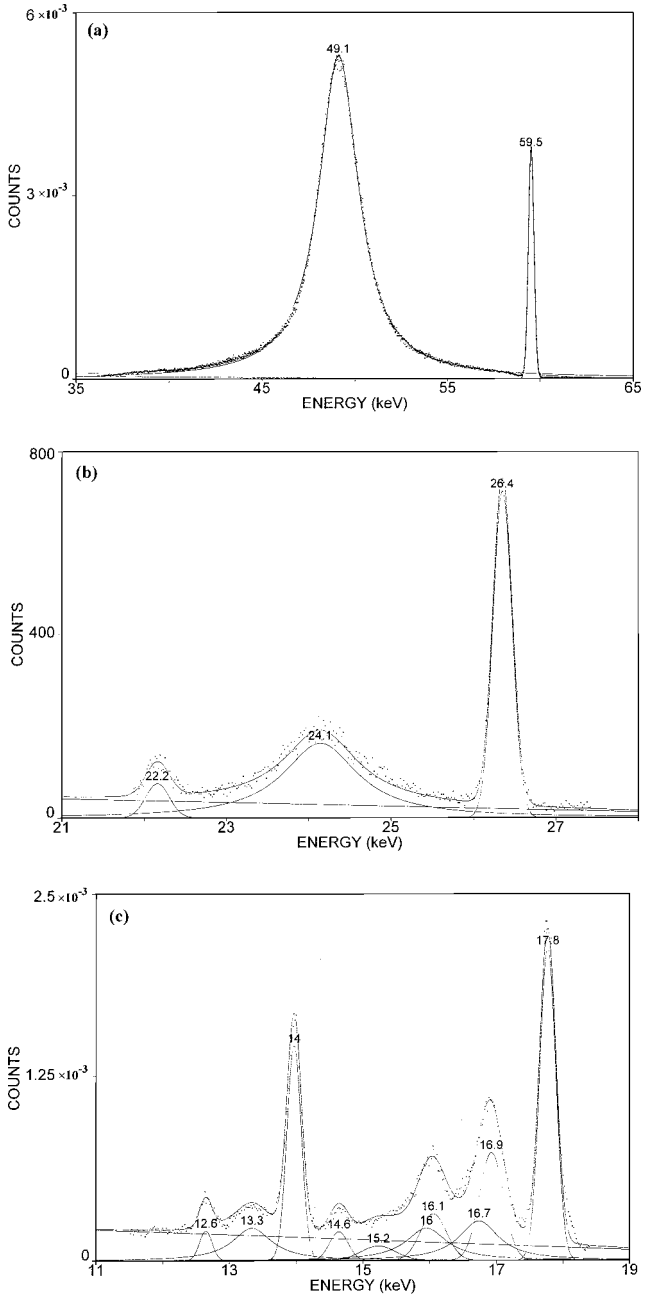

FIG. 1. Measured and fitted spectra for photons scattered through 145° by Cu. Resolved peaks are also indicated. (a) Scattering of 59.54-keV photons. (b) Scattering of 26.36-keV photons. (c) Scattering of 17.75- and 13.95-keV photons.

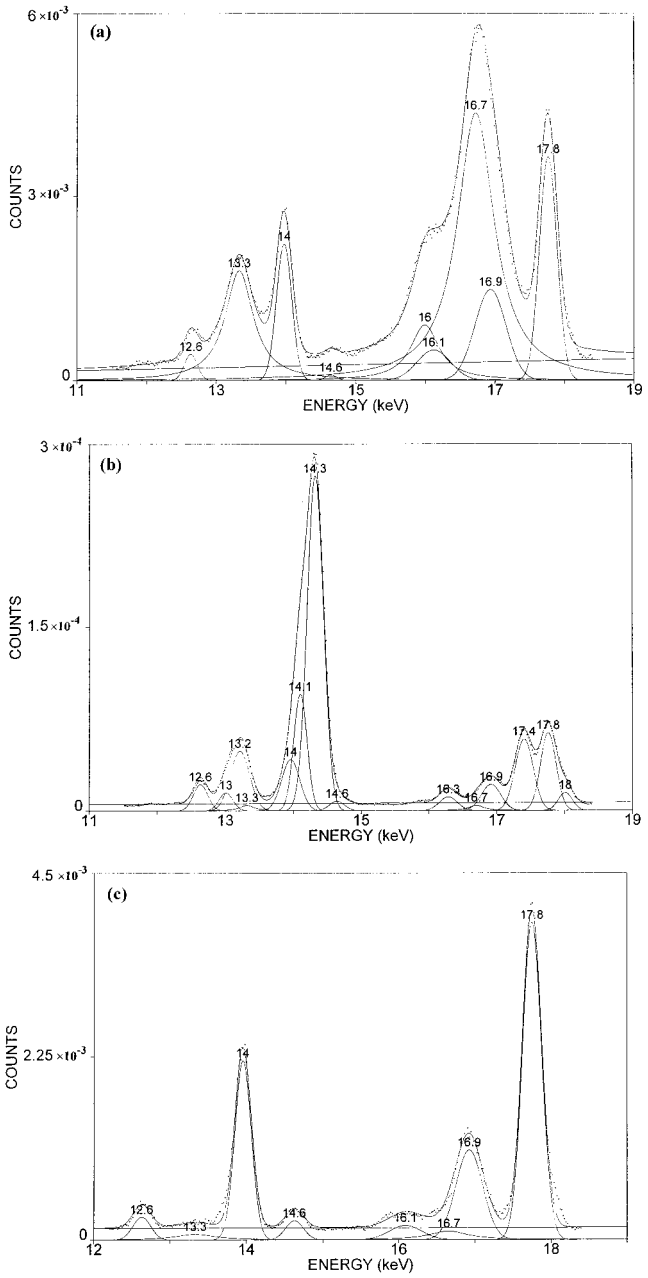

FIG. 2. Measured and fitted spectra of 17.75- and 13.95-keV photons scattering through 145° by (a) Al, (b) In, and (c) Ta. Resolved peaks are also indicated.

beryllium window. The source holder and target were positioned on a horizontal track, the arrangement being engineered to ensure negligible play of the source and scatterer. Each setting was checked to ensure that the source and target were adjusted to the same horizontal plane. The reproducibility of the short source-target and target-detector locations (less than 7 and 12 cm, respectively) were checked for each target by monitoring the count rates following repeated (3 times or more) removal and replacement of the scatterer; the maximum variation in count rate was less than 1%.

Foils of Cu, Zn, Zr, Nb, Mo, Ag, Cd, In, Sn, Ta, and W (Aldrich Chemical Company Inc.) of better than 99.9% purity were used as targets. The thickness of targets ranged from 0.05 to 0.25 mm, corresponding for most target elements at the 59.54-keV photon energy to thicknesses of less than one mean free path (MFP). However, for the same range of thickness as cited above, at the lower photon energies, the number of MFPs increased significantly. The differential scattering cross sections of interest were determined by comparing count rates with those obtained from Al foils of similar mean free paths.

Evaluation of differential scattering cross-sections has been based upon the relationship

$$\frac{d\sigma_{\mathrm{el}}}{d\Omega}=\left\langle\frac{d\sigma_T}{d\Omega}\right\rangle[F(x,Z=13)]^2\,\frac{I_{\mathrm{el}}}{I_{\mathrm{Al}}}\,\frac{n_{\mathrm{Al}}}{n_{\mathrm{el}}}\,\frac{T_{\mathrm{Al}}}{T_{\mathrm{el}}},$$

where $d\sigma_{\mathrm{el}}/d\Omega$ represents the differential coherent-scattering cross section. $d\sigma_T/d\Omega=r_e^2/2(1+\cos^2\theta)$ is the

differential Thomson scattering cross section per electron, with r_e the classical electron radius. $F(x,Z=13)$ is the atomic form factor for Al at the photon momentum transfer $x=\sin(\theta/2)/\lambda$, with λ the wavelength (in angstroms) of the incident radiation. $I_{\rm el}$ and $I_{\rm Al}$ are the count rates of elastic scattering photopeaks for the target element and Al respectively, while $n_{\rm el}$ and $n_{\rm Al}$ are the number of scattering centers per unit volume, with $n=(N_A\rho/A)$, where N_A refers to Avogadro's number, A is the atomic weight of the scattering medium, and ρ is its physical density. $T_{\rm el}$ and $T_{\rm Al}$ account for absorption incurred by the incoming and the scattered photon beam in traversing the target and Al respectively, where T is given by

$$T=\frac{\sin\phi}{\mu(1+\sin\phi)}\left\{1-\exp\left[-\mu t\left(\frac{1}{\sin\phi}+1\right)\right]\right\},$$

where $\phi=(\theta-\pi/2)$, μ is the applicable linear attenuation coefficient, and θ is the scattering angle. Values have been adopted from measurements previously performed by this group [23]. The estimated error 0 (10%) arises mainly from the values of μ (4–6%) and the counting statistics (2–4%). In the case of the 26.36-keV photons the estimated error may reach ~15% due to the poorer counting statistics that were obtained.

III. RESULTS AND DISCUSSION

The γ-ray spectrum from the different elements showed various peaks including scattered peaks (coherent and incoherent), fluorescence peaks, sum peaks, and Ge escape peaks. Figure 1 shows three energy regions of interest from the spectrum for a Cu sample for a 145° scattering angle: Fig. 1(a) relates to data obtained at the scattering of 59.54-keV photons, Fig. 1(b) to the scattering of 26.36-keV photons, and Fig. 1(c) to the scattering of photons of energies of 17.75 and 13.95 keV.

The elastic scattered peaks of 59.54 and 26.36 keV were clearly resolved from their Compton peaks for all elements. Direct measurement of the intensity was obtained by measuring the area under the peak. However, for the group of elements Ag, In, and Sn the low-intensity 26.36-keV elastic-scattering peaks were located at the shoulders of the high-intensity fluorescence peaks of the corresponding elements. Due to the dominance of the highly intense fluorescence peaks in this region, the 26.36-keV peaks can be assessed only when the spectrum was expanded.

A comparison of the energy region of the spectrum in which the elastic-scattering peaks of 17.75 and 13.95 keV were located for the elements Al, In, and Ta for a 145° scattering angle is shown in Figs. 2(a), 2(b), and 2(c), respectively. This region of the spectrum is more complex because of the significant overlap of these two peaks with their Compton peaks especially for low-Z elements. In addition, there is the overlap of Ge escape peaks that come into effect for some elements, notably In [see Fig. 2(b) peaks at 13, 13.2, 14.1, 14.3, 16.3, 17.4, and 18 keV) and Sn. A small fluorescence ($L\alpha$) peak from the Pb shielding at 12.6 keV is also visible in Fig. 2. This peak was also visible in Fig. 1(c).

For cases of the overlapping peaks (the 13.95- and 17.75-keV regions), the area under the elastic-scattering peaks were determined after the various peaks were resolved using a peak fitting program (PEAK FIT, V.4, Jandel Scientific). The program uses an enhanced version of the Levenburg-Marquardt nonlinear minimization algorithm for peak fitting. All nonlinear fitting algorithms are limited in the sense that the minimization must proceed iteratively from some initial set of parameter estimates. In this case the scattering spectrum of interest covers the energy region from approximately 10 to 60 keV. For a peak fitting analysis, the spectrum was divided into regions, each of which contains the elastic-scattering peaks and its overlapping neighbors. The data for each region were analyzed separately by the program. This was done by specifying the number of known peaks in the region, their centers, and width. The program then performs the final fitting of the data. For peak fitting, the errors are due mostly to the counting statistics, consistent with the magnitude of the peak. As discussed earlier, the associated errors are estimated to be in the range 2–4%. The residuals define the accuracy of the fit and reveal the existence of possible hidden peaks that may not have been identified. In our analysis, the residuals were insignificant since we have already accounted for all the known peaks listed, as illustrated in Figs. 1 and 2.

For the 11 target atoms under study a comparison has been made between experimentally obtained values of differential elastic-scattering cross sections and interpolated values of relativistic form factors (RFFs) [24], modified form factors (MFFs) [25], more recent theoretical predictions based upon modified form factors with anomalous scattering correction (ACMFFs), and relativistic form factors with anomalous scattering correction (ACRFFs), the latter two sets of predictions being available from tabulations of Kissel and Bergstrom [26]. The comparisons with ACMFF and ACRFF predictions are presented in Tables I–VIII. The difference between the ACMFF and ACRFF data for both the experimental and theoretical results in the case of the 59.54-keV photons was significant. The comparison between the experimental and theoretical results for both models is presented separately in Tables I and II. As for the case of the lower-energy photons presented in Tables III–VIII, the difference between the two models for both the experimental and theoretical results was insignificant (less than 3%). Figures 3–6 provide a graphical representation of some of these data and the relevant theoretical predictions. The quoted experimental values are the mean of results obtained for foils of two different thicknesses. With absorption being taken into account, the individual results have been found to be in every case within $\pm 3\%$ of each other [2]. For each photon energy, change in scattering angle, from 145° to 165°, has provided only small variation in the momentum transfer x, yielding small changes in the values of $(d\sigma/d\Omega)$; this has provided an ability to monitor potential sensitivity to variation in scattering angle. In the process of normalizing results against Al, the applicable atomic form factors for Al were assumed to be those corresponding to the particular formalism against which experimental data were compared.

No experimental values were obtained at the photon energy 17.75 keV for the targets Zr and Mo and 26.36 keV for the target Cd, this being due to the fact that the respective peaks were in each case significantly dominated by detected x-ray fluorescence from the targets. In other cases partial

TABLE I. Comparison of the experimental values of the differential elastic-scattering cross section of various elements obtained with 59.54-keV photons at scattering angles 145°, 154°, and 165°. The corresponding theoretical values were obtained using MFFs with anomalous scattering corrections (ACMFFs) from the tabulations of Kissel and Bergstrom [26]. Figures in parentheses below the elements refer to respective K edges in keV [27].

Element (keV)	$\frac{d\sigma}{d\Omega}$ (b/sr)					
	$\theta=145°$ $x=4.58$ Å^{-1}		$\theta=154°$ $x=4.68$ Å^{-1}		$\theta=165°$ $x=4.76$ Å^{-1}	
	Expt.	Theor.	Expt.	Theor.	Expt.	Theor.
Cu (8.979)	0.113	0.114	0.105	0.119	0.113	0.124
Zn (9.659)	0.126	0.123	0.131	0.129	0.132	0.134
Zr (17.998)	0.286	0.307	0.286	0.313	0.279	0.320
Nb (18.986)	0.317	0.338	0.298	0.345	0.305	0.352
Mo (20.000)	0.346	0.373	0.348	0.380	0.344	0.387
Ag (25.514)	0.510	0.586	0.496	0.597	0.510	0.608
Cd (26.711)	0.589	0.636	0.548	0.648	0.558	0.661
In (27.940)	0.629	0.687	0.596	0.701	0.604	0.715
Sn (29.200)	0.735	0.761	0.717	0.778	0.720	0.794
Ta (67.417)	0.707	0.768	0.762	0.787	0.743	0.805
W (69.525)	0.834	0.872	0.775	0.895	0.798	0.917

TABLE II. Comparison of the experimental values of the differential elastic-scattering cross section of various elements obtained with 59.54-keV photons at scattering angles 145°, 154°, and 165°. The corresponding theoretical values were obtained using RFFs with anomalous scattering corrections (ACRFFs) from the tabulations of Kissel and Bergstrom [26]. Figures in parentheses below the elements refer to respective K edges in keV [27].

Element (keV)	$\frac{d\sigma}{d\Omega}$ (b/sr)					
	$\theta=145°$ $x=4.58$ Å^{-1}		$\theta=154°$ $x=4.68$ Å^{-1}		$\theta=165°$ $x=4.76$ Å^{-1}	
	Expt.	Theor.	Expt.	Theor.	Expt.	Theor.
Cu (8.979)	0.109	0.107	0.101	0.112	0.108	0.116
Zn (9.659)	0.122	0.116	0.125	0.121	0.127	0.125
Zr (17.998)	0.275	0.285	0.274	0.290	0.267	0.296
Nb (18.986)	0.305	0.314	0.286	0.320	0.292	0.325
Mo (20.000)	0.333	0.347	0.333	0.352	0.329	0.358
Ag (25.514)	0.492	0.545	0.476	0.554	0.489	0.562
Cd (26.711)	0.566	0.592	0.526	0.601	0.534	0.611
In (27.940)	0.605	0.640	0.572	0.651	0.689	0.662
Sn (29.200)	0.707	0.689	0.688	0.702	0.689	0.715
Ta (67.417)	0.680	0.652	0.652	0.663	0.636	0.675
W (69.525)	0.802	0.744	0.744	0.759	0.764	0.773

TABLE III. Comparison of the experimental values of the differential elastic-scattering cross section of various elements obtained with 26.36-keV photons at scattering angles 145°, 154°, and 165°. The corresponding theoretical values were obtained using MFFs with anomalous scattering corrections (ACMFFs) from the tabulations of Kissel and Bergstrom [26]. Figures in parentheses below the elements refer to respective K edges in keV [27].

	$\frac{d\sigma}{d\Omega}$ (b/sr)					
Element	$\theta=145°$ $x=2.03$ Å^{-1}		$\theta=154°$ $x=2.07$ Å^{-1}		$\theta=165°$ $x=2.11$ Å^{-1}	
(keV)	Expt.	Theor.	Expt.	Theor.	Expt.	Theor.
Cu (8.979)	1.19	1.16	1.10	1.19	1.21	1.22
Zn (9.659)	1.27	1.29	1.31	1.33	1.38	1.36
Zr (17.998)	2.46	2.33	2.48	2.44	2.68	2.55
Nb (18.986)	2.56	2.38	2.56	2.50	2.86	2.61
Mo (20.000)	2.31	2.43	2.66	2.55	2.84	2.65
Ag (25.514)	1.82	1.95	2.19	2.02	2.34	2.08
Cd (26.711)		0.72		0.70		0.69
In (27.940)	1.64	1.57	1.59	1.57	1.53	1.57
Sn (29.200)	2.00	2.06	2.19	2.07	2.22	2.08
Ta (67.417)	10.50	12.53	10.64	13.08	11.84	13.57
W (69.525)	12.52	12.95	12.86	13.53	12.89	14.06

TABLE IV. Comparison of the experimental values of the differential elastic-scattering cross section of various elements obtained with 26.36-keV photons at scattering angles 145°, 154°, and 165°. The corresponding theoretical values were obtained using RFFs with anomalous scattering corrections (ACRFFs) from the tabulations of Kissel and Bergstrom [26]. Figures in parentheses below the elements refer to respective K edges in keV [27].

	$\frac{d\sigma}{d\Omega}$ (b/sr)					
Element	$\theta=145°$ $x=2.03$ Å^{-1}		$\theta=154°$ $x=2.07$ Å^{-1}		$\theta=165°$ $x=2.11$ Å^{-1}	
(keV)	Expt.	Theor.	Expt.	Theor.	Expt.	Theor.
Cu (8.979)	1.18	1.15	1.10	1.18	1.20	1.20
Zn (9.659)	1.26	1.28	1.30	1.31	1.37	1.35
Zr (17.998)	2.45	2.30	2.47	2.41	2.67	2.51
Nb (18.986)	2.54	2.35	2.55	2.46	2.85	2.57
Mo (20.000)	2.29	2.39	2.64	2.51	2.83	2.61
Ag (25.514)	1.80	1.92	2.18	1.98	2.33	2.05
Cd (26.711)		0.69		0.67		0.66
In (27.940)	1.63	1.53	1.58	1.52	1.52	1.53
Sn (29.200)	1.99	2.01	2.17	2.02	2.21	2.03
Ta (67.417)	10.42	12.29	10.57	12.82	11.76	13.29
W (69.525)	12.43	12.70	12.78	13.26	12.80	13.77

TABLE V. Comparison of the experimental values of the differential elastic-scattering cross section of various elements obtained with 17.75-keV photons at scattering angles 145°, 154°, and 165°. The corresponding theoretical values were obtained using MFFs with anomalous scattering corrections (ACMFFs) from the tabulations of Kissel and Bergstrom [26]. Figures in parentheses below the elements refer to respective K edges in keV [27].

	$\frac{d\sigma}{d\Omega}$ (b/sr)					
Element	$\theta=145°$ $x=1.37$ Å^{-1}		$\theta=154°$ $x=1.40$ Å^{-1}		$\theta=165°$ $x=1.42$ Å^{-1}	
(keV)	Expt.	Theor.	Expt.	Theor.	Expt.	Theor.
Cu (8.979)	2.77	2.57	3.07	2.70	2.77	2.81
Zn (9.659)	3.23	2.70	3.22	2.84	3.40	2.97
Zr (17.998)		1.27		1.25		1.23
Nb (18.986)	2.54	2.69	2.66	2.71	2.56	2.73
Mo (20.000)		3.49		3.53		3.67
Ag (25.514)	6.74	7.05	6.68	7.19	6.16	7.33
Cd (26.711)	7.87	7.81	7.27	7.98	6.85	8.15
In (27.940)	9.45	8.58	9.02	8.79	8.13	8.99
Sn (29.200)	9.72	9.35	9.74	9.61	8.55	9.85
Ta (67.417)	22.73	24.98	25.31	26.11	25.44	27.16
W (69.525)	27.11	25.73	19.77	26.87	25.12	27.93

TABLE VI. Comparison of the experimental values of the differential elastic-scattering cross section of various elements obtained with 17.75-keV photons at scattering angles 145°, 154°, and 165°. The corresponding theoretical values were obtained using RFFs with anomalous scattering corrections (ACRFFs) from the tabulations of Kissel and Bergstrom [26]. Figures in parentheses below the elements refer to respective K edges in keV [27].

	$\frac{d\sigma}{d\Omega}$ (b/sr)					
Element	$\theta=145°$ $x=1.37$ Å^{-1}		$\theta=154°$ $x=1.40$ Å^{-1}		$\theta=165°$ $x=1.42$ Å^{-1}	
(keV)	Expt.	Theor.	Expt.	Theor.	Expt.	Theor.
Cu (8.979)	2.76	2.57	3.06	2.68	2.76	2.80
Zn (9.659)	3.21	2.69	3.20	2.83	3.39	2.95
Zr (17.998)		1.25		1.23		1.21
Nb (18.986)	2.53	2.67	2.65	2.68	2.55	2.70
Mo (20.000)		3.46		3.49		3.53
Ag (25.514)	6.72	7.00	6.66	7.14	6.13	7.27
Cd (26.711)	7.83	7.75	7.24	7.92	6.82	8.08
In (27.940)	9.42	8.52	8.98	8.73	8.10	8.92
Sn (29.200)	9.68	9.29	9.70	9.54	8.52	9.78
Ta (67.417)	22.65	24.77	25.21	25.88	25.34	26.91
W (69.525)	27.00	25.51	19.69	26.62	25.02	27.67

TABLE VII. Comparison of the experimental values of the differential elastic-scattering cross section of various elements obtained with 13.95-keV photons at scattering angles 145°, 154°, and 165°. The corresponding theoretical values were obtained using MFFs with anomalous scattering corrections (ACMFFs) from the tabulations of Kissel and Bergstrom [26]. Figures in parentheses below the elements refer to respective K edges in keV [27].

	$\frac{d\sigma}{d\Omega}$ (b/sr)					
Element	$\theta=145°$ $x=1.07$ Å^{-1}		$\theta=154°$ $x=1.10$ Å^{-1}		$\theta=165°$ $x=1.12$ Å^{-1}	
(keV)	Expt.	Theor.	Expt.	Theor.	Expt.	Theor.
Cu (8.979)	4.42	3.52	4.04	3.70	4.14	3.87
Zn (9.659)	4.33	3.68	4.49	3.86	5.50	4.02
Zr (17.998)	5.93	6.63	6.94	6.77	5.27	6.90
Nb (18.986)	6.99	7.56	7.29	7.73	7.63	7.90
Mo (20.000)	7.53	8.51	4.74	8.72	14.31	8.92
Ag (25.514)	12.50	13.34	11.38	13.86	12.92	14.32
Cd (26.711)	12.50	14.27	13.05	14.85	13.15	15.38
In (27.940)	14.67	15.16	15.76	15.82	13.99	16.41
Sn (29.200)	15.93	16.02	15.85	16.75	15.23	17.40
Ta (67.417)	38.65	37.08	41.22	38.63	44.49	40.06
W (69.525)	32.86	37.66	33.08	39.21	103.82	40.63

TABLE VIII. Comparison of the experimental values of the differential elastic-scattering cross section of various elements obtained with 13.95-keV photons at scattering angles 145°, 154°, and 165°. The corresponding theoretical values were obtained using RFFs with anomalous scattering corrections (ACRFFs) from the tabulations of Kissel and Bergstrom [26]. Figures in parentheses below the elements refer to respective K edges in keV [27].

	$\frac{d\sigma}{d\Omega}$ (b/sr)					
Element	$\theta=145°$ $x=1.07$ Å^{-1}		$\theta=154°$ $x=1.10$ Å^{-1}		$\theta=165°$ $x=1.12$ Å^{-1}	
(keV)	Expt.	Theor.	Expt.	Theor.	Expt.	Theor.
Cu (8.979)	4.41	3.51	4.03	3.69	4.14	3.86
Zn (9.659)	4.32	3.67	4.48	3.84	5.49	4.01
Zr (17.998)	5.91	6.60	6.92	6.74	5.26	6.87
Nb (18.986)	6.97	7.53	7.27	7.70	7.61	7.86
Mo (20.000)	7.51	8.47	4.73	8.69	14.28	8.88
Ag (25.514)	12.47	13.30	11.36	13.81	12.89	14.27
Cd (26.711)	12.49	14.21	13.03	14.79	13.11	15.32
In (27.940)	14.64	15.10	15.73	15.76	13.95	16.34
Sn (29.200)	15.89	15.96	15.82	16.68	15.19	17.33
Ta (67.417)	38.56	36.90	41.12	38.43	44.38	39.84
W (69.525)	32.79	37.47	33.00	39.00	103.56	40.42

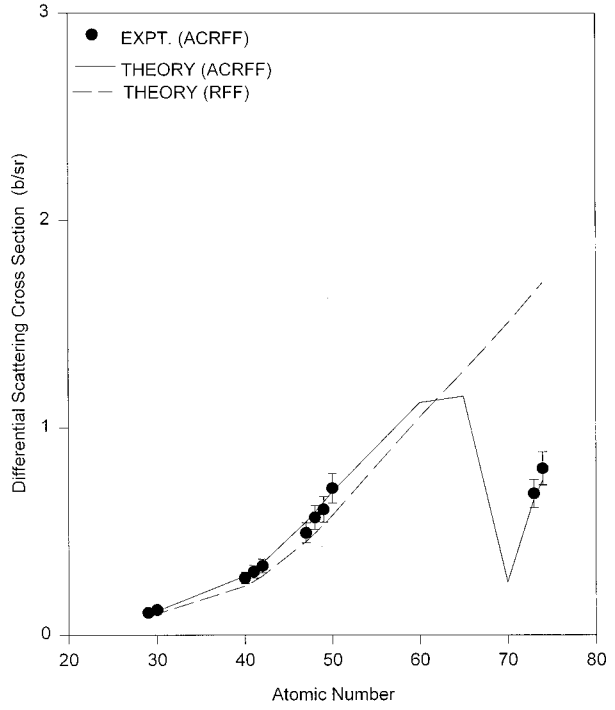

FIG. 3. Comparison of experimental and theoretical differential cross sections (b/sr) for elastic scattering at $x = 4.58$ Å^{-1} as a function of atomic number.

overlap between the elastic-scattering peaks and the intense fluorescence lines were resolvable, one instance being that for the 26.36-keV line for the targets Ag, Sn, and In.

The experimental results yield broad accord with predicted magnitudes, better accord being found at higher-x values for low-Z targets and at lower-x values for high-Z targets. The experimental data are generally higher than RFF and MFF predictions further away from the absorption edge, but lower than those in the immediate vicinity of the absorp-

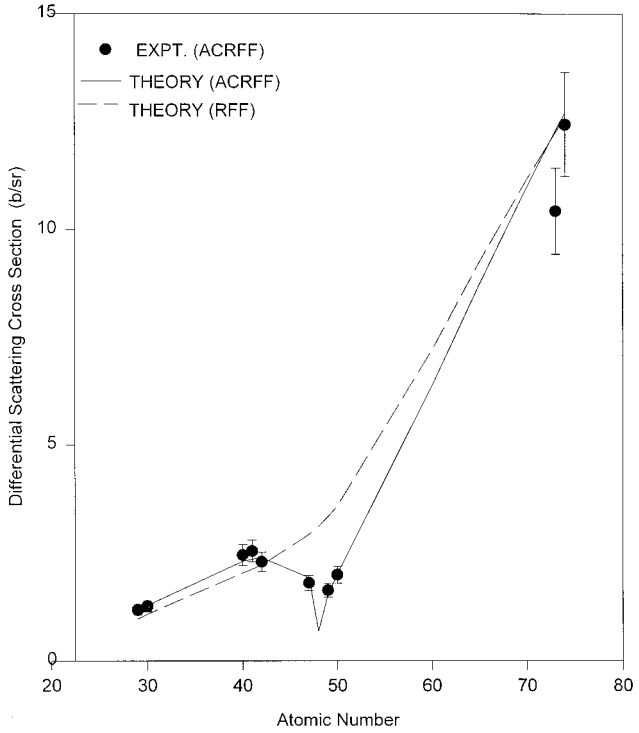

FIG. 4. Comparison of experimental and theoretical differential cross sections (b/sr) for elastic scattering at $x = 2.03$ Å^{-1} as a function of atomic number.

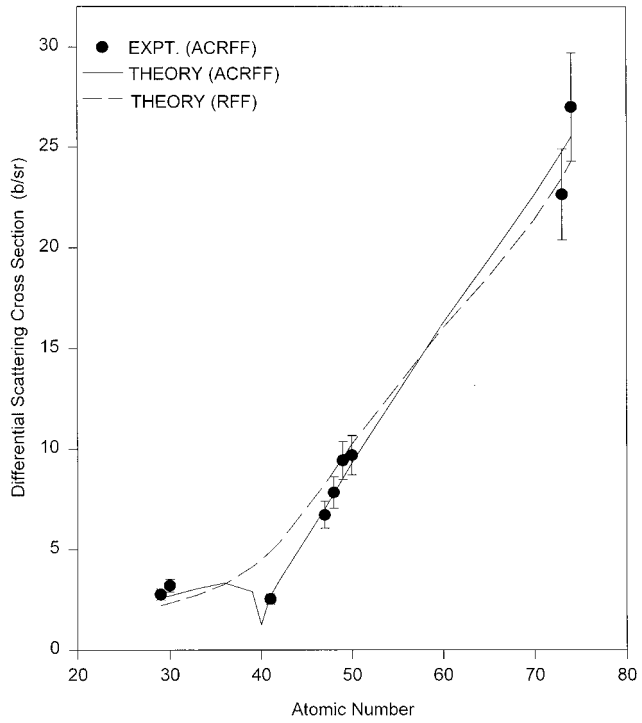

FIG. 5. Comparison of experimental and theoretical differential cross sections (b/sr) for elastic scattering at $x = 1.37$ Å^{-1} as a funcion of atomic number.

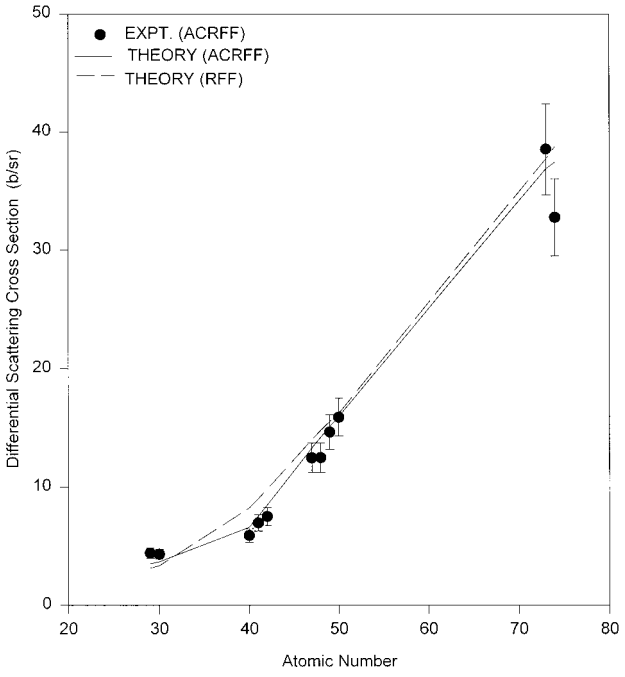

FIG. 6. Comparison of experimental and theoretical differential cross sections (b/sr) for elastic scattering at $x = 1.07$ Å^{-1} as a function of atomic number.

tion edge. When incorporating anomalous corrections, the agreement between the experimental and theoretical predictions (ACMFFs and ACRFFs) were greatly enhanced, especially in the vicinity of the absorption edge. In detailed comparisons significant discrepancies are found between both MFF and RFF predictions and experiment. In particular, experimental values were in excess of 50% lower than associated predictions for 59.54-keV photons on targets of W and Ta, 26.36-keV photons on targets of Ag, Sn, and In, and 17.75-keV photons on Nb. In all of these cases the respective atomic absorption *K* edges were close to the cited incident photon energies. When a comparison is made with ACMFF and ACRFF predictions, the experimental results show significantly improved agreement. For instance, ACRFF predictions and measured scattering cross sections of 59.54-keV photons from atoms of Ta and W agree to within 10%. A similar result is obtained for the scattering of 17.75-keV photons from Nb (being in the vicinity of the absorption *K* edge), the discrepancy between experiment and ACRFF predictions reduced to within 6%. In general, the ACRFF predictions provide the best agreement with experimental results and the significant improvements that are obtained are particularly clear near and below the *K* edges. Fluctuations and an unexpectedly large discrepancy are noted between theory and experiment for incident photons of 13.95 keV on targets of Mo and W. In particular, the observed scattering intensity for Mo and W was significantly larger than predicted at the scattering angle of 165°. At 154°, the experimental cross sections are substantially smaller than the corresponding predictions, with the discrepancy being more pronounced for the element Mo. Clearly, the occurrences are not in accord with the general trend of the experimental data. The reasons behind the appearance of these particular features and primarily that for Mo are still under investigation. One possibility in the case of the observed elevation in intensity is Bragg reflection within this range of scattering angles.

ACKNOWLEDGMENTS

The authors acknowledge research grants from the National Science Foundation (Grant No. INT891 3055) and R&D 123 3416 2201 provided by the Universiti Sains Malaysia. Particular thanks are due to Richard Pratt of the University of Pittsburgh and Lynn Kissel and Paul Bergstrom of Lawrence Livermore National Laboratory for making available theoretical predictions and providing the impetus for this continuing cooperative research program.

[1] W. Chittwattanagorn, S. Kwaengsobha, J. Jarasrangsichol, K. Rachdawanpong, and P. Oungmanee, Nucl. Instrum. Methods Phys. Res. A **225**, 75 (1987).
[2] D. A. Bradley, C. S. Chong, A. A. Tajuddin, A. Shukri, and A. M. Ghose, Phys. Rev. A **41**, 5974 (1990).
[3] L. Kissel, B. Zhou, S. C. Roy, S. K. Sen Gupta, and R. H. Pratt, Acta Crystallogr., Sect. A: Found. Crystallogr. **51**, 271 (1995).
[4] L. Kissel and R. H. Pratt, Acta Crystallogr., Sect. A: Found. Crystallogr. **46**, 170 (1990).
[5] B. Zhou, R. H. Pratt, S. C. Roy, and L. Kissel, Phys. Scr. **41**, 495 (1990).
[6] N. Govinda Nayak, K. Siddappa, K. M. Balakrishna, and N. Lingappa, Phys. Rev. A **45**, 4490 (1992).
[7] S. K. Ghose, M. Ghose, S. S. Nandi, A. C. Nandi, and N. Choudhuri, Phys. Rev. A **41**, 5869 (1990).
[8] P. P. Kane, G. Basavaraju, S. M. Lad, K. M. Varier, L. Kissel, and R. H. Pratt, Phys. Rev. A **36**, 5626 (1987).
[9] C. Bui and M. Milazzo, Nuovo Cimento D **11**, 655 (1989).
[10] M. L. Garg, R. R. Garg, F. Henrich, and D. Heimermann, Nucl. Instrum. Methods Phys. Res. B **73**, 109 (1993).
[11] G. Basavaraju, P. P. Kane, L. D. Kissel, and R. H. Pratt, Phys. Rev. A **49**, 3664 (1994).
[12] G. Basavaraju, P. P. Kane, S. M. Lad, L. Kissel, and R. H. Pratt, Phys. Rev. A **51**, 2608 (1995).
[13] M. Schumacher and A. Stoffregen, Z. Phys. A **283**, 15 (1977).
[14] S. S. Nandi, R. Dutta, and N. Chaudhuri, J. Phys. B **20**, 4027 (1987).
[15] K. M. Varier and M. P. Unnikrishnan, Nucl. Instrum. Methods Phys. Res. A **280**, 428 (1989).
[16] S. Puri, B. Chand, D. Mehta, M. L. Garg, N. Singh, and P. N. Trehan, Nucl. Instrum. Methods Phys. Res. B **111**, 209 (1996).
[17] J. Eichler and S. de Barros, Phys. Rev. A **32**, 789 (1985).
[18] F. Smend and H. Czerwinski, Z. Phys. D **1**, 139 (1986).
[19] K. Siddappa, N. G. Nayak, K. M. Balakrishna, N. Lingappa, and Shivaramu, Phys. Rev. A **39**, 5106 (1989).
[20] E. Casnati, C. Baraldi, and A. Tartari, Phys. Rev. A **42**, 2627 (1990).
[21] S. Erzeneoglu, Y. Kurucu, R. Durak, and Y. Sahin, Phys. Rev. A **51**, 4628 (1995).
[22] C. S. Chong, A. A. Tajuddin, A. Shukri, and D. A. Bradley, Radiat. Phys. Chem. **47**, 689 (1996).
[23] A. A. Tajuddin, C. S. Chong, A. Shukri, T. Bandyopadhyay, and D. A. Bradley, Appl. Radiat. Isot. **46**, 113 (1995).
[24] J. H. Hubbell and I. Overbo, J. Phys. Chem. Ref. Data **8**, 69 (1979).
[25] D. Shaupp, M. Schumacher, F. Smend, P. Rullhusen, and J. H. Hubbell, J. Phys. Chem. Ref. Data **12**, 467 (1983).
[26] L. Kissel and P. M. Bergstrom, tabulations available from http://www-phys.llnl.gov/V DIV/scattering/fftab angle.html
[27] C. M. Lederer and V. S. Shirley, *Table of Isotopes*, 7th ed. (Wiley-Interscience, New York, 1978).